npj | Clean Water

www.nature.com/npjcleanwater

ARTICLE OPEN

Check for updates

# Fouling behavior of wavy-patterned pore-filling membranes in reverse electrodialysis under natural seawater and sewage effluents

Jiyeon Choi[1,4,5]✉, Won-Sik Kim[1,2,4], Han Ki Kim[1], Seung Cheol Yang[1,3], Ji-Hyung Han[1], Yoon Cheul Jeung[1] and Nam Jo Jeong[1,5]✉

Reverse electrodialysis (RED) generates electricity from a mixture of seawater and river water. Herein, patterned membranes consisting of ultra-thin pore-filling membranes (16-μm thick) were used to determine whether the RED system operates steadily when using natural underground seawater and sewage effluent and if the membranes become polluted by various foulants. The flat stack performances, comprising flat membranes and woven-type spacers, were compared with those of the pattern stack, comprising patterned membranes with mirror-imaged wavy lines. The pattern stack clearly reduced the pressure drop and maintained the power within 40% of the initial value, and the flat stack significantly increased to 3 bar inside the sewage effluent and decreased the power to 20% of the initial value. Both anion and cation exchange-surface membranes showed organic fouling and scaling, with more significant fouling in the flat stack. The patterned membranes used here provide a powerful solution to reduce fouling inside RED stacks.

*npj Clean Water* (2022)5:6 ; https://doi.org/10.1038/s41545-022-00149-2

## INTRODUCTION

The depletion of fossil fuels and their greenhouse effect have increased interest in non-polluting energy resources. In this regard, reverse electrodialysis (RED), which is the fundamental principle of a membrane-based electrochemical energy system that generates electricity by mixing seawater and river water, has been investigated. Recently, the electricity generated by RED systems using salinity gradients was theoretically estimated to be only 625 TWh/yr, which was equivalent to 3% of global electricity consumption at the time, owing to several physical and environmental constraints[1]. The RED stacks that are used in this system primarily consist of an alternating series of cation exchange membranes (CEMs), anion exchange membranes (AEMs), electrolytes with different salinities (i.e., at high and low concentrations, HC and LC, respectively), and a pair of electrodes as well as electrode rinse solutions (ERSs) that are capable of converting ionic currents into electric currents via the reversible redox reaction (Fig. 1(a)).

Several studies have been conducted to investigate the main parameters that affect the performance of REDs, including membrane structures[2–9], process conditions[10–12], and stack designs[13]. Recently, several well-organized reviews have comprehensively discussed related issues ranging from materials to practical pilot tests[14–16]. Specifically, it has been observed that feed waters help to improve the performance of REDs given that they influence the electromotive driving force and internal resistance of the REDs. Hence, owing to their accessibility, artificial NaCl solutions with concentrations of 0.5 and 0.017 M are generally used as feed solutions. However, to establish sustainable power generation as an environmentally friendly alternative energy source, it is necessary to further develop RED processes not only for model solutions, but also for practical conditions.

Based on the property of Gibbs' free energy associated with mixing, RED can be operated irrespective of the water source considered, provided there is a sufficient salinity gradient for the ion-exchange membranes (IEMs)[15]. Natural seawater, brine, river water, and wastewater are among the available water sources. Recently, there have been reports on the applications of various combinations of these influents and conditions in practical pilot-scale RED stacks[11,12]. However, when using natural influents for RED stacks, fouling can become a critical problem.

Multivalent ions, such as magnesium and sulfate ions, which are naturally dissolved in water, have negative impacts in terms of IEM scaling. Meanwhile, AEMs are mainly affected by organic fouling and biofouling. To reduce fouling, various strategies by which materials and operating processes can be improved have been reported, e.g., the periodic reversal of influents, air sparging[17], and the use of $CO_2$-saturated water[18].

Profiled membranes that can improve spacer geometries can serve as an alternative solution to minimizing the fouling phenomenon as well as the pressure drop inside RED stacks. Vermaas et al.[8] first fabricated profiled membranes using straight lines for RED stacks via the hot-press method and reported its fouling behavior under natural feed waters[17,19]. However, the number of studies on the functioning of RED stacks under natural feed waters (e.g., natural seawater and sewage effluent) are limited[17–21]. Supplementary Table 1 summarizes representative fouling studies using RED stacks.

The patterned membranes used in this study have several features. First, they use ultra-thin pore-filling membranes with a thickness of 16 μm as supporting membranes. These membranes act as inert substrates to provide mechanical stability, and an electrolyte polymer that fills the pores of the substrate affords ion conductivity. Our group has developed a pore-filling membrane[3,4]

[1]Korea Institute of Energy Research, Jeju Global Research Center, 200 Haemajihean-ro, Gujwa-eup, Jeju-si, Jeju-do 63357, Republic of Korea. [2]Jeju Energy Corporation, 18-4, Cheongsa-ro 1-gil, Jeju-si, Jeju-do, Republic of Korea. [3]Changwon National University, Department of Materials Convergence and System Engineering, 20 Changwondaehak-ro, Uichang-gu, Changwon-si, Gyeongsangnam-do 51140, Republic of Korea. [4]These authors contributed equally: Jiyeon Choi, Won-Sik Kim. [5]These authors jointly supervised: Jiyeon Choi, Nam Jo Jeong. ✉email: jychoi@kier.re.kr; njjeong@kier.re.kr

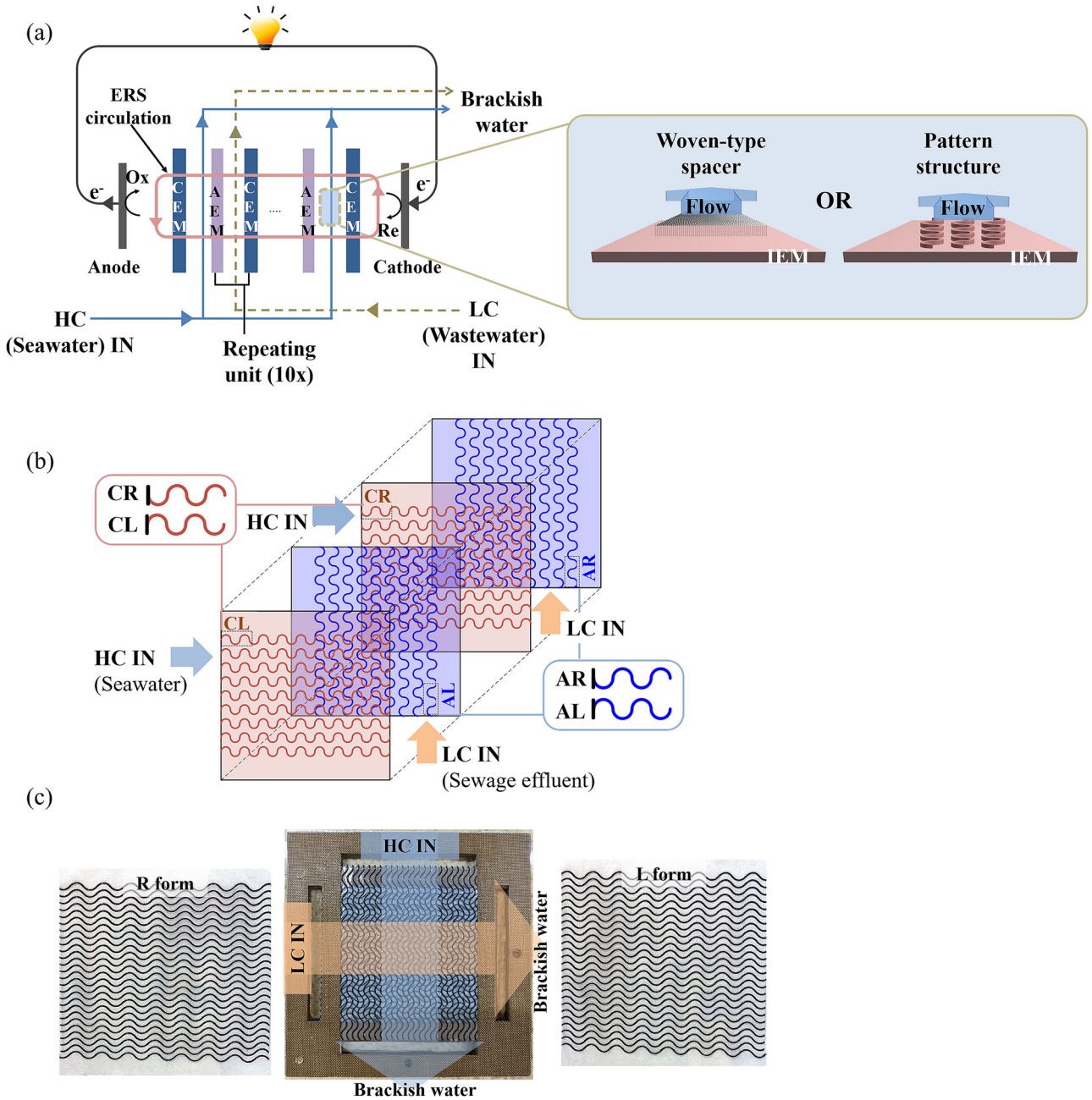


**Fig. 1 Schematic of the RED process when using a woven-type spacer or patterned membrane, the method for stacking the patterned membranes with their mirror images, and photographic image of the cross-flow stacked patterned membranes. a, b** Show schematic of the RED process and the method for stacking the patterned membranes with their mirror images, respectively. **c** Shows photographic image of the cross-flow stacked patterned membranes (L and R form) used in this study. HC and LC indicate high and low concentrations of the electrolyte, respectively.

for RED systems. Second, instead of the hot-pressing method, they utilize different patterning methods with a dispenser-type printer that employs photocuring because the pattern structure cannot be hot-pressed on IEMs with a thickness of only 16 μm. Third, they apply designed wave patterns via a mirror image. Fourth, they fabricate heterogeneous patterned membranes with different chemical compositions[22]. To match the thickness of the spacer, the height of the patterned structure is set to 100 μm. Additionally, the pattern was designed to be shaped like a mirror image to prevent the overlap of the pattern structure with the stacked ion-exchange membranes with opposite charges. We classified the patterns into L- and R-types, depending on whether the ends of the lines point to the left or right, respectively. As shown schematically in Fig. 1(b), AEMs are designated "AL" and "AR," and CEMs are designated "CL" and "CR." AL and AR are stacked with a CEM in between, and the CL and CR are stacked with an AEM in between. Figure 1(c) shows a photograph of the stacked-pattern membrane used in this study.

Our group focuses on the development of RED systems that can stably maintain high performance even under actual influent conditions, such as real seawater and sewage effluent. Unlike previous studies that evaluated the long-term performance by extending the intermembrane distance up to 800 μm (Supplementary Table 1), this study aimed to investigate the fouling behavior inside RED stacks using narrow intermembrane distances (~100 μm) and realistic influent conditions. We also investigated

whether the fouling of the stack was effectively reduced by using only patterned membranes and switching the flow direction of the inlet and outlet.

## RESULTS AND DISCUSSION

In this study, we investigated the performance of the RED stack using natural feed waters under actual environmental conditions. Particularly, we analyzed surface fouling after disassembling the flat and pattern stacks and distinguished between reversible and irreversible fouling on the membrane surfaces.

### Reversible fouling behavior through pressure drop

Figure 2 shows the results of the pressure drop over the flat and patterned stacks. For in situ cleaning, we manually switched the positions of the inlet and outlet tubes whenever the pressure rose over 1 bar, irrespective of the feed water (seawater or sewage). This switching was performed at least once a day on most days. As a result, detachable contaminants that were reversibly attached around the inlet were gradually washed away from the membrane surface; this is a more convenient process compared with air sparging and/or chemical cleaning given that no additional energy or chemical supplements were required[16]. The other advantage of this process was that the RED system continuously generated power because the switching process did not require a system shutdown.

For underground seawater, the pressure drop corresponding to the pattern stack increased significantly at a faster rate than that corresponding to the flat stack within the first 2 days of the experiment, and thereafter, it remained stable below 1 bar. This confirms the efficacy of the switching method (inlet and outlet) in minimizing the pressure drop. Although the pressure drop corresponding to the flat stack increased by more than 1 bar after 4 days, after switching, it further decreased to values below 1 bar. Additionally, regardless of the stacking arrangement, flat or pattern stacks, the seawater side operated stably at pressures below 2 bar. In particular, the pattern stack pressure remained below 2 bar for 14 days. In the control experiment using 3 and 0.1% NaCl solutions (Supplementary Fig. 1), no pressure drop was observed in the patterned stack, and the flat stack was confirmed to operate stably at 0.1 bar (3% NaCl) and 0.2 bar (0.1% NaCl).

As illustrated in Fig. 2b, the sewage effluent showed dramatic changes in the pressure drop. Compared with underground seawater (Fig. 2a), the inlet/outlet switching cycles associated with the sewage effluent were accelerated. For the flat stack, the pressure drop gradually increased to 1 bar within 24 h, and rapidly increased to 2 bar after 2 days. In the early stages of reversible foulant-accumulation (up to ~3 days), switching the inlet and outlet seemed to effectively remove foulants. However, after 3 days, this effect was no longer observed because high pressure was maintained on the 4th day, even after the inlet and outlet were switched. The operation was stopped after 5 days owing to the excessively high pressure. Although the patterned stack showed a similar trend with the sewage effluent, the pressure drop increased to a maximum of 2.2 bar after 5 days and then operated between the maximum and minimum values (2.2 and 0.7 bar, respectively) for a total of 14 days of operation. However, when the influent direction was switched, it was confirmed that the pressure drop fell below 1 bar.

These results indicate that patterned membranes are more advantageous in limiting the pressure drop owing to the absence of the woven-type spacer. Moreover, these results showed a significantly high pressure drop over a relatively short period of time owing to the narrower intermembrane distance of 100 μm compared with previously reported results on fouling[17–19], as summarized in Supplementary Table 1. Particularly, it has been reported that the theoretical pressure drop associated with uniform and laminar flow depends on the intermembrane distance[23].

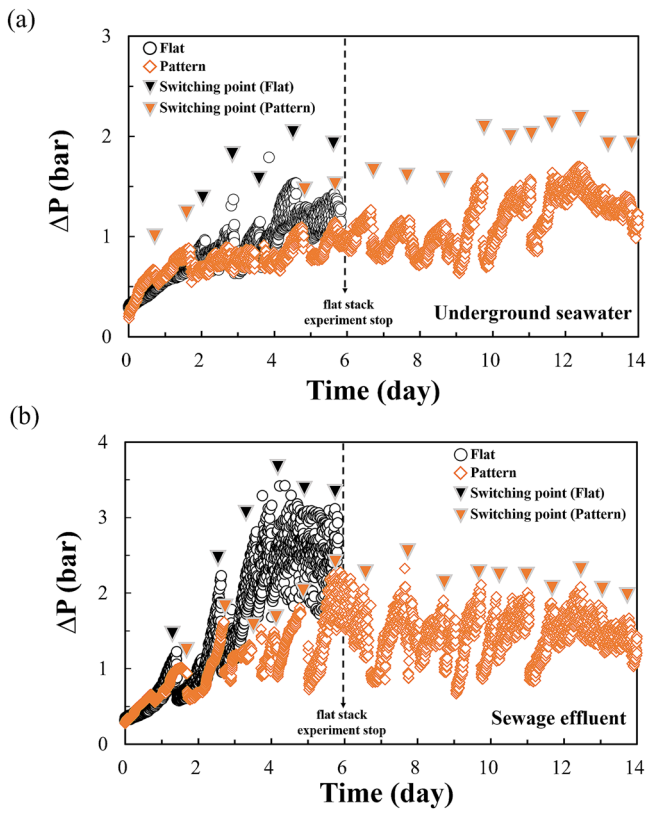


**Fig. 2 Pressure drop as a function of time. a, b** show pressure drop as a function of time at underground seawater side and at sewage effluent side. The inverted triangles indicate switching points.

### Change in electrochemical performance by fouling behavior

Results other than those corresponding to pressure drop were based on the operating period of the two stack systems and the characterization of samples that were collected after five days of operation. This was performed to compare the fouled phenomena associated with the patterned and flat stacks after operation for the same duration.

Figure 3 shows the open-circuit voltage (OCV) and normalized power, as functions of the number of days of operation measured during the continuous RED operation. The OCV corresponding to the flat stack decreased from 1.15 to 0.44 V, while that corresponding to the patterned stack remained stable in the

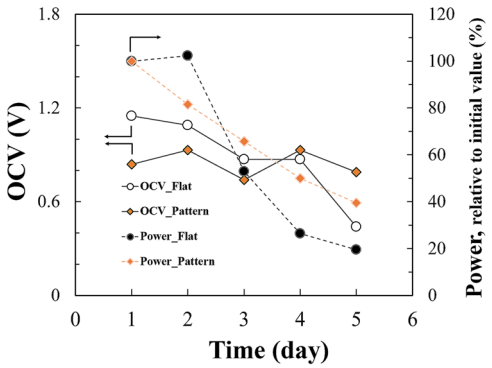


**Fig. 3 Measured OCV and power (%) as functions of operation time for 5 days.** The power was normalized to the initial value.

range 0.84–0.79 V for 5 days. Further, the normalized power in the flat stack also decreased to 20% relative to the initial power, whereas that in the patterned stack was maintained at 40%. Additionally, the OCV and power of the flat stack sharply declined after 3 days when the pressure drop corresponding to the sewage effluent side rapidly increased. This can be explained by an increase in membrane resistance (Table 2) and a decrease in apparent permselectivity (Supplementary Fig. 2). With artificial seawater and river water (0.5 and 0.017 M NaCl, respectively), the OCV values in the flat and patterned stacks were 1.23 and 1.25 V[22], and the apparent permselectivities were 0.88 and 0.84 at a flow rate of 30 mL/min, respectively (Supplementary Table 3). These slight differences were because poor mixing and severe concentration polarization were likely to occur in the patterned stack, compared to the flat stack, at a low flow rate[22]. According to the Nernst equation, various ion compositions and the concentration of multivalent ions also affect the OCV when the salinity ratios of feed waters are the same[24,25]. Moreover, according to Kingsbury et al.[26], the presence of natural organic matter (NOM) had a significant impact on the decrease of the OCV and corresponding reduction in the permselectivity; that is, the permselectivity decreased as the dissolved organic carbon (DOC) concentration increased in dilute feed water. As the charged organic foulants tend to adhere to the surface of the IEM, the surface charge may decrease, which in turn affects the permselectivity against counterions and co-ions[19]. Compared to the flat stack, the patterned stack was only slightly influenced by foulants (Fig. 2), thus the apparent permselectivity was maintained within the range of 60–70% for 5 days. For the flat stack, the rapid decrease in the OCV was attributed to serious fouling inside the stack. Subsequently, the power, which is dependent on the permselectivity and the total resistance (including the membrane resistance), also sharply decreased.

Table 1 summarizes the changes in the membrane resistance before and after the continuous RED process. In the case of the flat CEMs and AEMs, the membrane resistance was measured with the woven spacer in place. This allowed the investigation of its influence. It was observed that the membrane resistance of the flat CEMs increased from 0.49 to 0.54 Ω cm$^2$, while that of the flat AEMs increased from 0.55 to 0.67 Ω cm$^2$. These values were higher than those only measured with flat membranes (Supplementary Table 3). Regarding the patterned membrane, the resistance of its CEMs increased from 0.83 to 0.87 Ω cm$^2$, while that of its AEMs increased from 0.97 to 1.05 Ω cm$^2$. Compared with their pristine equivalents, the membrane resistance of the flat CEMs and AEMs with spacers increased by 10.2 and 21.8%, respectively, whereas that of the patterned CEMs and AEMs without spacers increased by 4.8 and 8.2%, respectively. This increase in membrane resistance suggests that charged molecules causing organic fouling were possibly trapped on the IEM surface. The flat stack with spacers showed a greater change in the ohmic resistance than the patterned stack. This observation can be attributed to excessive fouling caused by colloidal, scaling, and biological foulants because of the relatively large membrane area that was covered with non-conductive spacers. The decreased local-flow velocity around the spacer easily accumulated the foulants given that the geometry of the spacer affects the uniformity of the distribution of the feed water. Consequently, the decrease of the effective membrane area enhanced the membrane resistance and inhibited the power density.

**Table 1.** Change of membrane resistance before and after continuous reverse electrodialysis operation. The values with standard deviations were measured in triplicate at least.

| Ω·cm$^2$ | Flat with spacer | | Pattern | |
|---|---|---|---|---|
| | Pristine | Fouled | Pristine | Fouled |
| CEM | 0.49 ± 0.07 | 0.54 ± 0.03 | 0.83 ± 0.04 | 0.87 ± 0.04 |
| AEM | 0.55 ± 0.02 | 0.67 ± 0.03 | 0.97 ± 0.08 | 1.05 ± 0.03 |

### Visual inspection of irreversible fouled membranes

We evaluated the degree of fouling in the RED stack based on the IEM type and the use of a spacer. After continuous operation for 5 days and using underground seawater and sewage effluent as natural feed waters and assuming practical conditions, we disassembled the RED stacks to observe the degree of fouling of the membranes and spacers.

Representative photos of the fouled membranes and spacers are shown in Fig. 4, from which it is difficult to clearly distinguish between the inlet and outlet sides given that the flow direction was switched to reduce the extent of fouling inside the stack. However, the difference in the degree of fouling between the in/outlet and middle parts was significant. This is apparent from the FE-SEM images (Figs. 5 and 6).

After continuous operation for five days, there was a visual confirmation of significant fouling on the flat membranes and spacers, compared with the patterned membranes. Further, as shown in Fig. 4(a), the color of the AEM changed from slightly opaque white to reddish-brown. Furthermore, the color change of the patterned membrane was slightly less prominent than that of the flat membrane. It was also observed that more reddish-brown contaminants accumulated on the in/outlet sides than on the middle region. The spacer and patterned membrane changed to the same color because various foulants occupied the porous structures and surfaces along the pattern channels. The brown-red color indicated the presence of humic substances, which have negatively charged anionic polyelectrolytes that adsorb onto AEMs via electrostatic interaction[27]. Reportedly, humic substances constitute the predominant fraction of NOM, and they can be categorized as humic acid (HA), fulvic acid (FA), and humin[27]. The increase in their molecular weight via oxidative polymerization brings changes the color from light yellow (FA) to dark brown (HA) or black (humin)[27,28]. The brown color of the AEM did not change after washing via sonication, indicating irreversible fouling on the membrane owing to the chemisorption of humic substances.

As shown in Fig. 4(b), CEMs showed less severe coloration than AEMs. However, the accumulation of reddish-brown contaminants at the inlet and outlet regions was similar. The reddish-brown foulants were adsorbed on the surface via a physical means given that they could be easily removed via physical scratching. Meanwhile, AEMs are known to be more sensitive to organic foulants (e.g., HA, carbohydrates, and aromatic compounds). Such organic fouling primarily occurs on the surface and inside the membrane owing to electrostatic, van der Waals, and hydrophobic interactions[29]. Among the dissolved organic matter, NOM mainly consists of humic substances, which comprise more than 50% of DOC, and a range of compounds from small hydrophobic acids, proteins, and amino acids to larger HAs and FAs[30]. As shown in the Supplementary Table 4, the DOC values were much higher for the AEM (1.92 mg/L) than for the CEM (0.58 mg/L). The same tendency was observed for the patterned membranes (AEM = 0.68 mg/L and CEM = 0.26 mg/L).

The changes in the thickness indicated that fewer foulants were deposited in the middle region, whereas large amounts accumulated in the inlet region, which was particularly severe with the woven spacer (Supplementary Figs. 3 and 4). There was an obvious increase in the thickness at the inlet and outlet sides in the flat stack owing to the simultaneous occurrence of various fouling phenomena. The non-uniform fluid distribution caused by spacer filaments on the inlet side resulted in fouling both the flat membrane and the spacer. Subsequently, the increased internal residence time of the fluid created an environment that induced

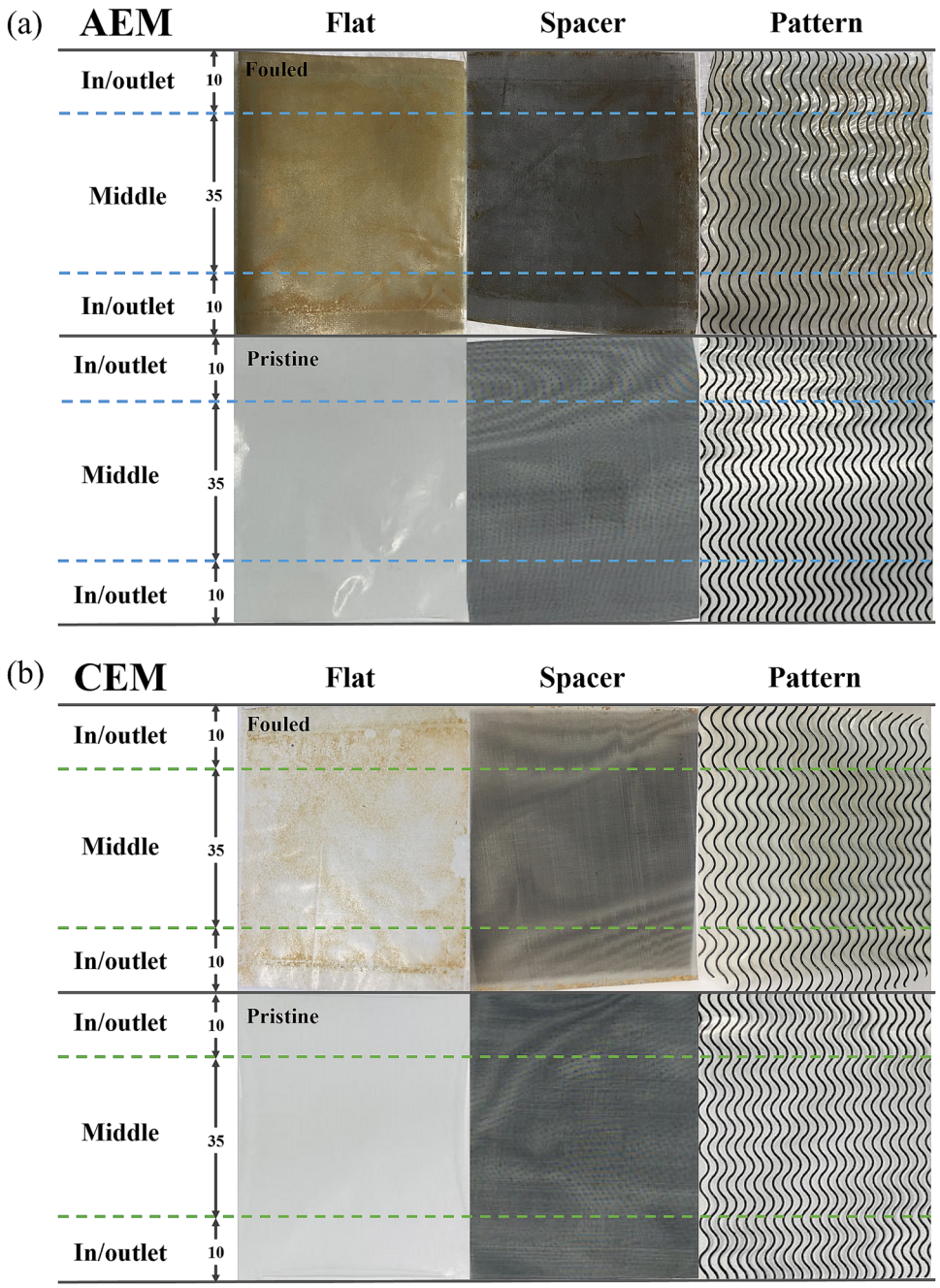


**Fig. 4 Photographs of flat, spacer, and patterned membranes before and after continuous RED operation for 5 days. a** Shows photographs of AEMs at the sewage effluent side. **b** Shows photographs of CEMs at the underground seawater side. The dimensions of the divided regions in this figure are in millimeters. The samples before and after continuous RED operation were classified into fouled or pristine.

concentration polarization and reversible fouling[30]. Based on the results of the change in the pressure drop, switching the direction of the feed water caused interference in the flow and eliminated reversible fouling, including those caused by colloidal silica and precipitated iron colloids, for a short period. However, after the formation of the cake- or gel-fouling layers on the membrane and spacer surfaces, the switching method did not affect the RED stacks with spacers in natural feed water even when monitored for longer periods. Thus, different methods such as chemical cleaning were required. On the contrary, there was less fouling in the patterned membrane because the fluid-flow was less obstructed, and the switching of the feed water direction was more effective. Therefore, these results indicate that patterned membranes can reduce membrane fouling, as well as support sewage effluents as practical influents in RED stacks for long-term operations.

### Microscopic visualization of irreversible fouled membranes

Figures 5 and 6 show the representative FE-SEM images corresponding to the CEMs and AEMs from the flat and patterned stacks, respectively. They also show clear differences in the membrane fouling depending on the type of membrane, and the influents (underground seawater and sewage effluent) that were in contact with the membranes.

As shown in Fig. 5, the fouling distributions in flat AEMs and CEMs were concentrated along the spacer geometry, and more fouling depositions accumulated when the membranes were in

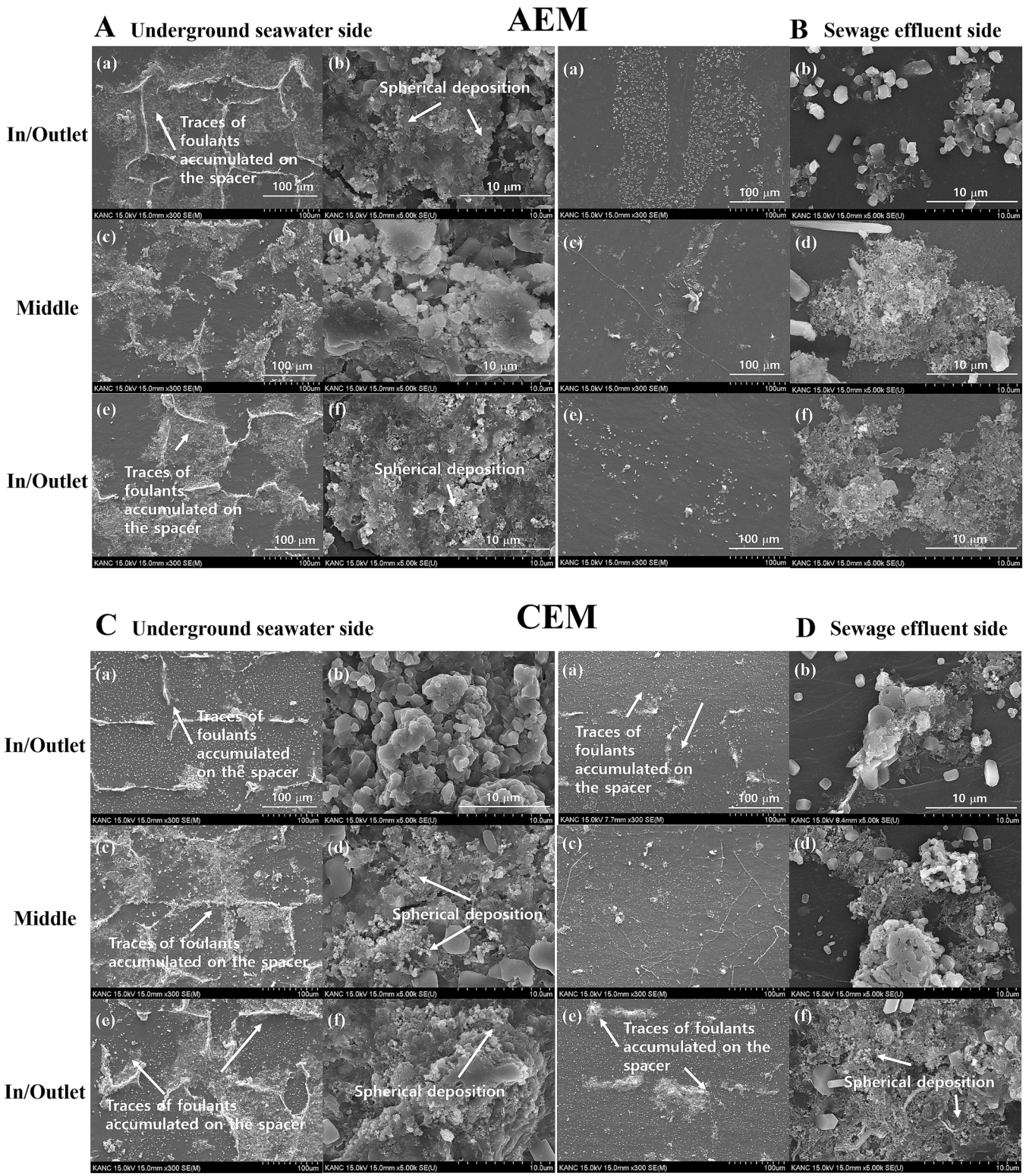


**Fig. 5 FE-SEM images of the flat membranes after continuous RED operation for 5 days. A**, **B** Show FE-SEM images of AEM at the underground seawater side and at the sewage effluent side. **C, D** Show FE-SEM images of CEM at the underground seawater side and at the sewage effluent side. Image magnifications: (a), (c), and (e) 300×; (b), (d), and (f) 1000×.

contact with the underground seawater than with sewage effluent. Moreover, the deposition of foulants in the spacer primarily occurred in areas with a stagnant flow velocity in the channel due to the obstructed flow by the spacer structure (Supplementary Fig. 4)[31]. Severe fouling, with a cake-like deposition, caused by particulate/colloidal foulants, occurred on the surface of the membranes in contact with underground seawater. Furthermore, particulate matter in natural waters, including a wide size range of colloids, forms a caked layer by accumulating after the initial blocking of pores[30]. Although the

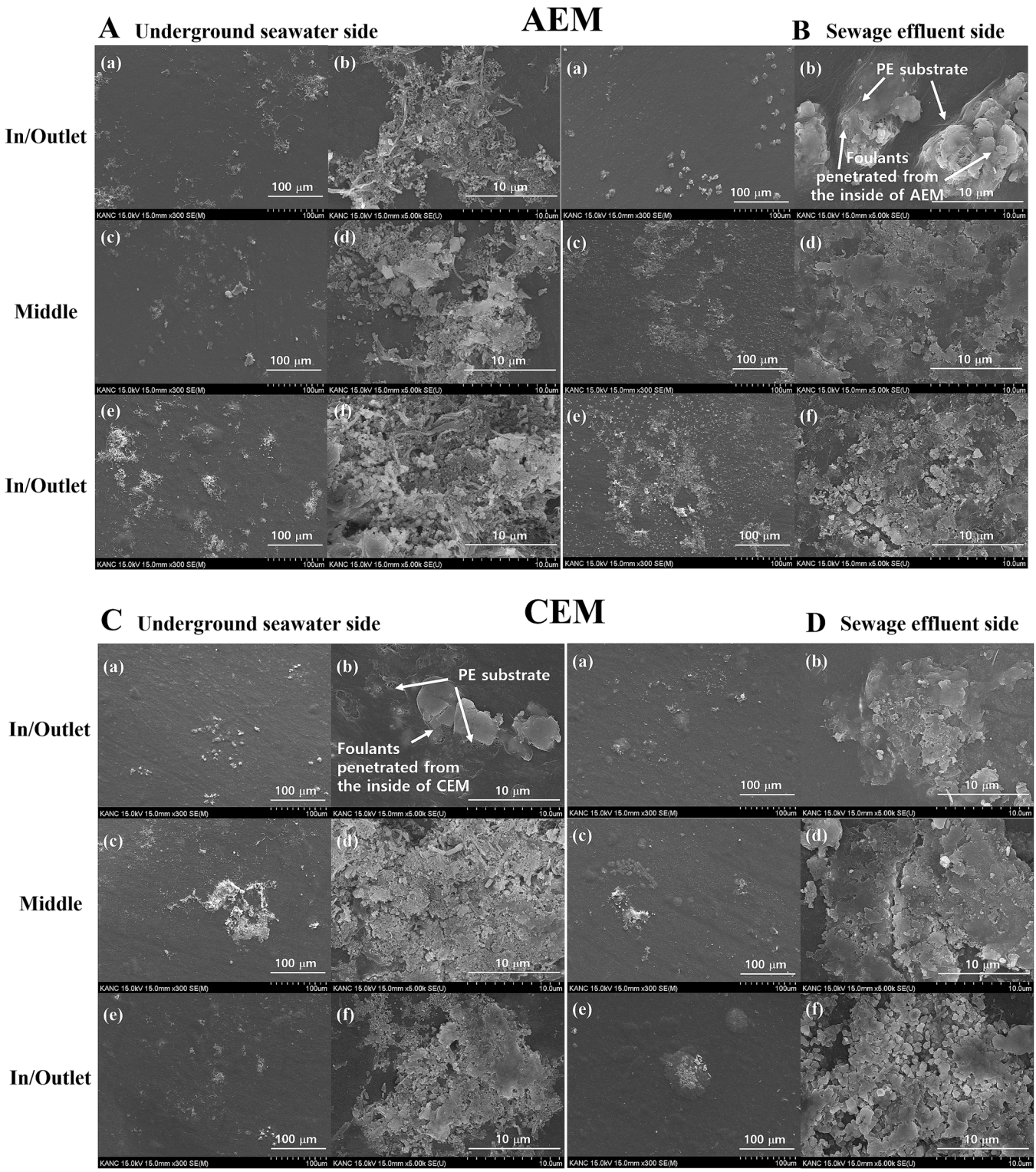


**Fig. 6 FE-SEM images of patterned membranes after continuous RED operation for 5 days. A**, **B** Show FE-SEM images of AEM at the underground seawater side and at the sewage effluent side. **C, D** Show FE-SEM images of CEM at the underground seawater side and at the sewage effluent side. Image magnifications: (a), (c), and (e) 300×; (b), (d), and (f) 1000×.

pore-filling membranes used in this study consisted of densely packed polyelectrolytes in porous polyolefin with pore sizes of 60 nm, aquatic colloidal solids under 1 μm can still be trapped inside or on the membranes. Moreover, this can become a form of precipitation, whose occurrence can be attributed to ionic species with charges that have polarity that is opposite those on the membranes. The AFM images in Supplementary Fig. 5 show extremely small spherical deposits in several places, unlike the images of the pristine AEM and CEM (Supplementary Fig. 6). In contrast, the membrane surfaces of the patterned AEMs and CEMs (Fig. 6) showed less fouling along the pattern channel (Fig. 4). Interestingly, for patterned membranes, the images showed the

**Table 2.** EDX results of the AEMs and CEMs of the patterned stack after continuous reverse electrodialysis operation for 5 days. The values with standard deviations were measured from three data points and the others correspond to a single data point.

| Atomic% | Patterned AEM | | Patterned CEM | |
|---|---|---|---|---|
| | Underground seawater side | Sewage effluent side | Underground seawater side | Sewage effluent side |
| Carbon | 54.4 ± 23.3 | 63.0 ± 5.6 | 44.6 ± 30.0 | 61.0 ± 5.4 |
| Oxygen | 34.0 ± 16.2 | 27.6 ± 5.5 | 38.8 ± 22.4 | 28.8 ± 3.4 |
| Sodium | 2.0 ± 1.0 | 3.1 ± 1.3 | 1.6 ± 1.6 | 1.7 ± 0.4 |
| Magnesium | 0.8 | 0 | 0.5 ± 0.5 | 0.4 ± 0.4 |
| Silicon | 0.9 ± 1.2 | 0.4 ± 0.2 | 2.73 | 0.3 ± 0.2 |
| Calcium | 0.6 ± 0.7 | 0.3 | 3.8 ± 4.5 | 1.8 ± 0.8 |
| Iron | 3.1 ± 2.6 | 1.0 ± 0.9 | 8.5 | 0.7 ± 0.7 |
| Sulfur | 1.7 ± 1.2 | 1.7 ± 1.0 | 6.1 ± 4.2 | 4.3 ± 1.1 |
| Phosphorus | 0.8 | 0.5 ± 0.4 | 0 | 0.9 |

formation of colloidal fouling or scaling inside the membrane as well as their spread outside the membrane (Fig. 6B(b) and 6C(b)). Generally, the type of fouling depends on the different functional groups of IEMs. Positively charged AEMs are prone to organic and biofouling, whereas negatively charged CEMs tend to attract scaling[15].

### Elemental composition and structural characterization of irreversible fouled membranes

Table 2 summarizes the elemental compositions of the fouled patterned membranes detected using EDX. The results corresponding to the flat stack are similar. This table represents the average values for the three regions: inlet, middle, and outlet. The standard deviations corresponding to the elements that were detected at only one of the three points were not calculated. The surfaces of the pristine membranes (AEM and CEM) primarily consisted of C, O, Na, S, and Cl originating from the polymeric electrolyte structure of the AEM, with quaternary ammonium cationic groups, and the CEM, with sodium sulfonate groups. However, the presence of elements corresponding to the components of the influent, and not those of the membrane, was confirmed in the fouled membranes.

The atomic concentrations (i.e., seawater and sewage in atomic %) of Ca (3.8 and 1.8), Mg (0.5 and 0.4), Fe (8.5 and 0.7), and S (6.1 and 4.3) on the CEM surface were much higher than those on the AEM surface. Specifically, Ca (0.6 and 0.3), Mg (0 and 0), Fe (3.1 and 1.0), and S (1.7 and 1.7) were measured on the AEM surfaces. Multivalent cations, such as Ca and Mg, were detected on the CEM surface owing to its negatively charged surface. As shown in Table 2, these elements were also the main components in the seawater and sewage compartments. Particularly, a high atomic concentration of S was detected owing to the functional groups of the CEM. The S content of CEM was approximately 2–3 times higher than that of AEM. Generally, scaling by inorganic ions ($Ca^{2+}$ and $Mg^{2+}$) usually occurs in CEMs because of the negatively charged groups. Ions dissolved in water, such as sulfates, carbonates, and phosphates, precipitated in the form of calcium carbonates, calcium phosphates, or magnesium sulfates, etc., under the influence of the pH of the solution, and these precipitates settled on or in the membrane[29] (Supplementary Fig. 7). Iron oxide and its derivatives, including its hydrate form, are reddish in color[32]. As seen in Fig. 4, the CEM surface was covered with reddish foulants, which were assumed to be iron oxides. Although the atomic concentrations of Ca, Mg, S, and P corresponding to AEM were lower than those corresponding to CEM, membrane scaling owing to the presence of multivalent ions could still occur in the AEMs at a neutral pH. Moreover, colloidal fouling in the form of colloidal silica, iron oxide, and clay minerals was mainly observed on the AEM surface owing to the negatively charged surface of the colloids. Higher concentration of other elements such as Si (0.9 and 0.4 atomic%) and Fe (3.1 and 1.0 atomic%) were detected in the AEM in contact with seawater and sewage effluent, than in the CEM, except at some positions in the latter. From the FE-SEM (Figs. 5 and 6) and AFM (Supplementary Fig. 5) results, it could be estimated that the spherical foulants comprised particulate/colloidal fouling. The fouling layer on AEM possibly consisted of organic and inorganic ion precipitates, indicating the presence of silicate $SiO_2$, $CaCO_3$, and $Mg(OH)_2$ sediments[33].

To confirm the changes in the functional groups on the membranes, attenuated total reflectance Fourier transform infrared (ATR-FTIR) analysis was performed on the specimens before and after fouling (Fig. 7). Although the characteristic elements were identified through EDX, it was difficult to deduce the structure of the contaminants attached to the membrane surfaces. Particularly, the functional groups of the IEM and organic foulants were similar. Thus, it was difficult to perform deconvolution to confirm changes in specific peaks. However, we could deduce the chemical structures of the foulant mixtures via the changes observed in the fingerprint region (650–1,350 $cm^{-1}$), including inorganic foulants, such as $Fe_2O_3$, $SiO_2$, and $Al_2O_3$, that are involved in scaling[30]. We assigned the ATR-FTIR spectra based on these compounds.

In AEM, only minimal changes were observed at the peaks. These changes could be attributed to the organic fouling of the entire area. However, a new peak that could be attributed to the characteristic adsorption of C = S, was observed at 2097 $cm^{-1}$ [34]. Peaks in the range 1257–1205 $cm^{-1}$ are indicative of the C–O band in aromatic alcohol compounds such as HA and FA. Therefore, the new peaks at 1078 and 1031 $cm^{-1}$ could be attributed to the stretching vibrations of the C–O– and Si–O bonds corresponding to polysaccharides or polysaccharide-like components[35] and silica colloids, respectively. Additionally, in CEM, a peak in the range 2965–3000 $cm^{-1}$, corresponding to the O–H of a carboxylic acid, hydrogen bonded to oxygen in water, or other carboxylic groups, was observed[36]. The weak peaks in the 905–830 $cm^{-1}$ region for both AEMs and CEMs could be ascribed to the binding of iron oxides and their derivatives, which resulted in a mixture of red and yellow foulants[32]. Further, Al–O–OH and Si–O–Al bonding can be assigned at 940 and 1011 $cm^{-1}$ [32]. The peaks at 1143, 1081, and 1133 $cm^{-1}$ indicated the presence of foulants such as iron oxide and iron sulfate.

## CONCLUSIONS

We investigated the effect of reducing fouling using patterned IEM based on changes in pressure drop and membrane resistance, and characterized the surface of the fouled membranes. A 14-day continuous RED process, using natural underground seawater and

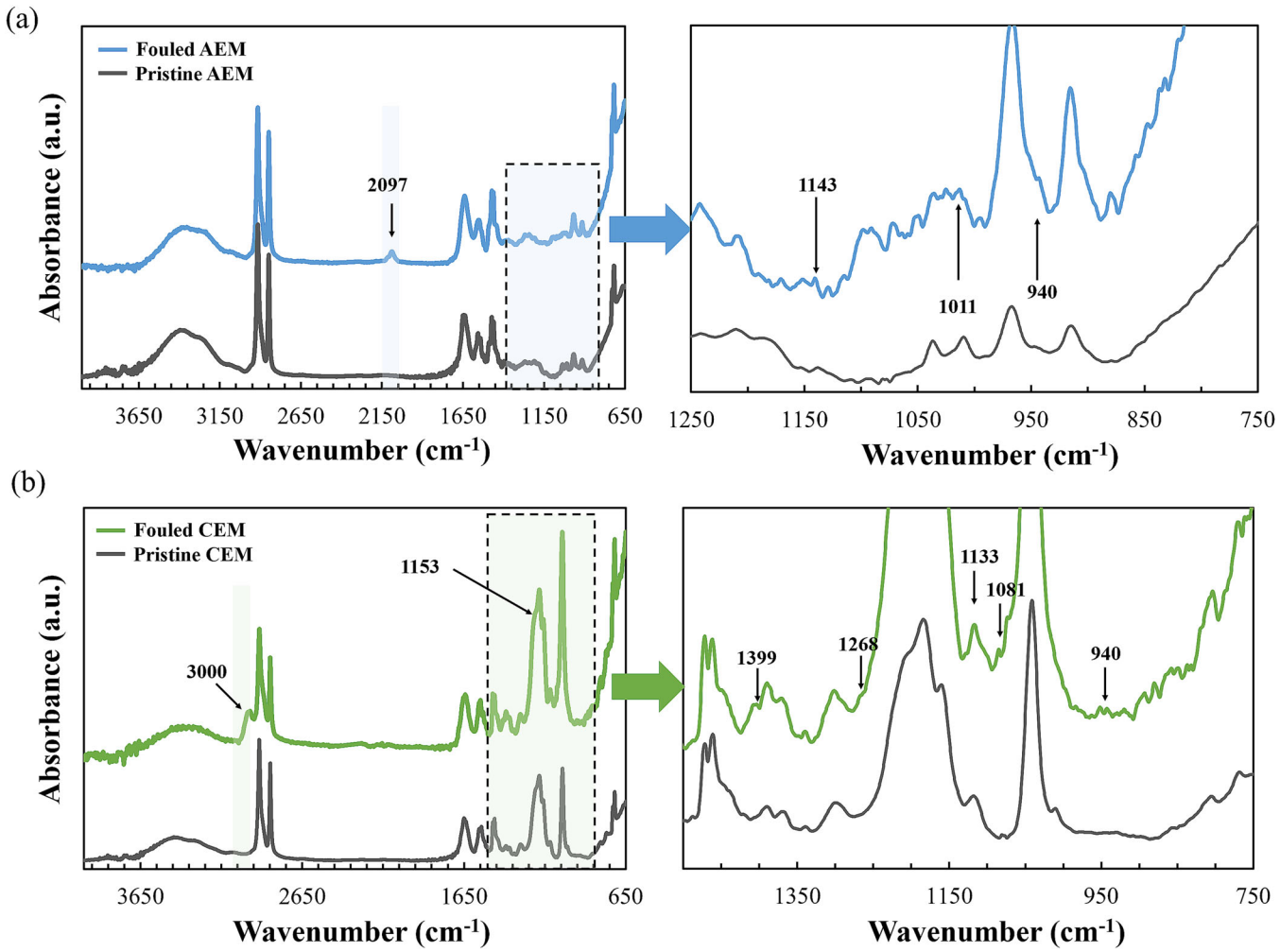


**Fig. 7 ATR-FTIR spectra of the pristine and fouled flat membranes after continuous RED operation. a, b** Show ATR-FTIR spectra of AEM and CEM.

sewage effluent as natural feed waters, was conducted for patterned membranes with an intermembrane distance of 100 µm. The pattern stack clearly reduced the pressure drop and maintained the power within 40% relative to the initial value, whereas the flat stack with sewage effluent significantly increased the pressure to 3 bar and decreased the power to 20% relative to the initial value. Moreover, switching the flow direction of the feed water in the inlet and outlet was an effective cleaning method by which pressure drop was decreased for a short duration. In particular, the accumulation of foulants was severe in the lattice portion of the spacer and in the inlet and outlet regions of the flat stack. Further, owing to the spacer geometry, there was a stagnant flow velocity as well as non-uniform fluid distribution in the RED stack, and severe fouling was observed at the inlet region. In contrast, the patterned membranes were evenly covered with foulants throughout the flow channel, and in terms of the color changes in the AEMs, severe organic fouling owing to the accumulation of HA was observed. Additionally, it was considered that the patterned membrane used in this study created a uniform fluid-flow environment that could reduce fouling in the RED stack under actual conditions. The possibility of long-term operation, while maintaining the performance of the RED stack was also demonstrated. Therefore, the patterned membranes used in this study, with an aggressive and practical cleaning strategy are expected to provide a powerful solution that can be employed to reduce fouling inside RED stacks, while maintaining performance, despite the narrow intermembrane distance.

**Table 3.** Configuration of the reverse electrodialysis stacks used in this study.

| | Flat stack | Pattern stack |
|---|---|---|
| Membrane | KIER membrane | KIER membrane |
| Membrane type | Flat | Patterned with wave line |
| Compartment support | Woven-type spacer | Patterned structure |
| Open area (%) | 46.4 | 75.0[a] |
| Intermembrane distance (µm) | 100 (spacer thickness) | 100 (pattern height) |

[a]Calculated value.

## METHODS

### Materials

For the pore-filling membrane, a microporous polyethylene (PE) substrate was purchased from W-scope (Japan) and used as a support for the AEM and CEM. According to the supplier information, the porosity, pore size, and thickness of this PE substrate were 43%, 60 nm, and 16 µm, respectively. Sodium dodecylbenzenesulfonate (SDBS) and

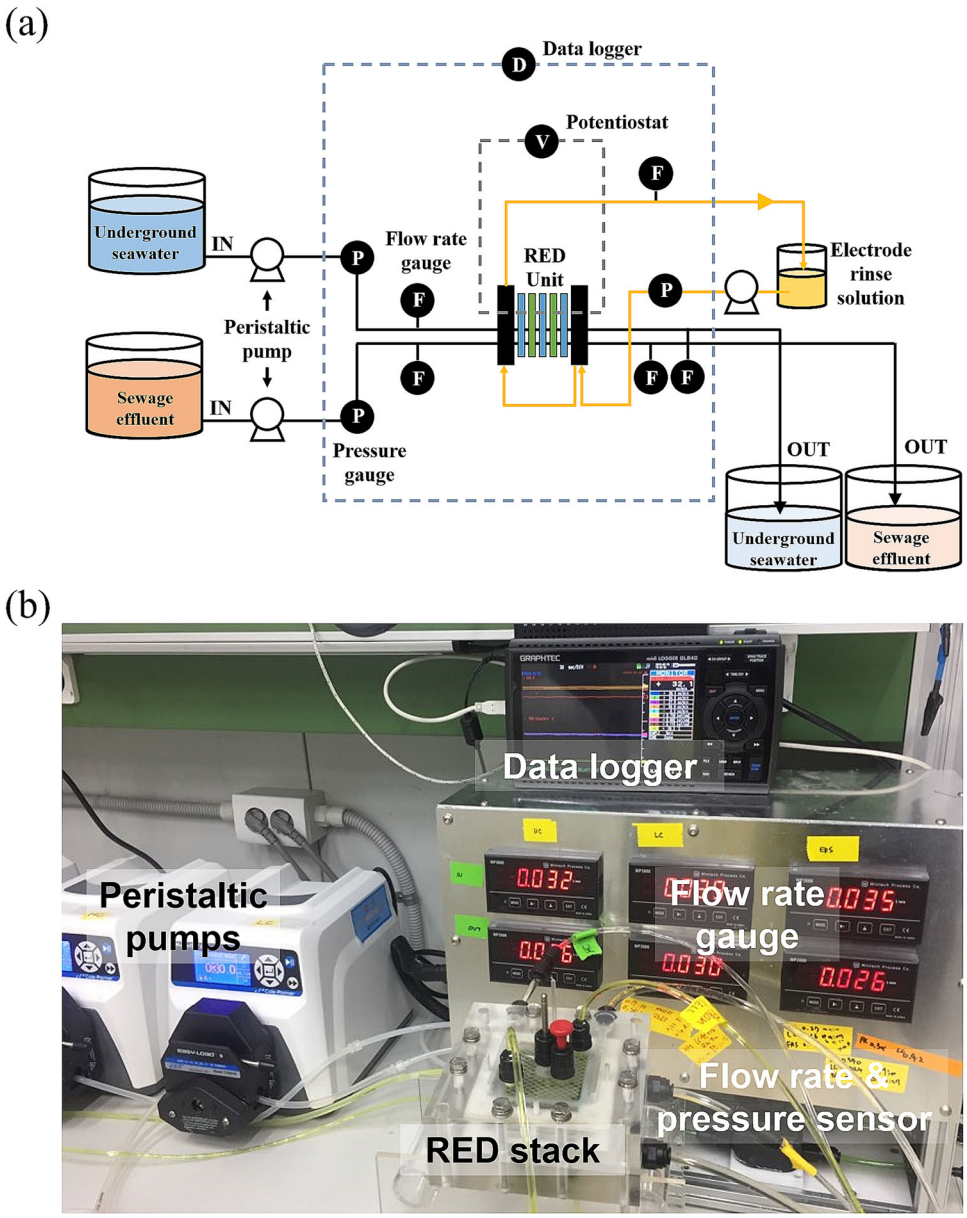


**Fig. 8 Schematic representation of the experimental set-up and photographic image of the actual configuration for the RED process.** **a** Shows simplified schematic representation of the experimental set-up. **b** Shows photographic image of the actual configuration for the RED process.

2-hydroxy-2-methylpropiophenone (Darocur 1173) were purchased from TCI (Japan). For the AEM and CEM, (3-acrylamidopropyl)trimethylammonium chloride (75 wt% in water, ATAC, KJ Chemical co., Japan) and 2-acrylamido-2-methyl-1-propanesulfonic acid sodium salt solution (50 wt% in water, AMPS-Na, Toagosei, Japan) were used as cationic and anionic monomeric electrolytes, respectively. Piperazine diacrylamide (PDA) was purchased from Richest group (China) for use as a crosslinker. To pattern the membranes, photo-curable inks (FM-200) were purchased from Evertech. (South Korea). For ERS, potassium ferricyanide (II) and potassium ferrocyanide trihydrate (III) were purchased from Daejung Chemicals & Metals co. (South Korea). All chemicals were used without further purification.

## Membranes

The flat pore-filling membranes (AEM and CEM) used in this study were fabricated by four major steps: pretreatment, electrolyte impregnation, photo-polymerization, and polishing[4]. To hydrophilize the microporous PE substrate, it was immersed in a 0.1 wt% solution of SDBS in deionized water for 1 min and subsequently dried with hot air at 70 °C. For the AEM electrolyte solution, ATAC, PDA, and a photoinitiator (Darocur 1173, 10 wt % in methanol) were used in a dry weight ratio of 12:1:0.1. For the CEM electrolyte, AMPS-Na, PDA, and a photoinitiator (Darocur 1173, 10 wt% in methanol) were used in the same ratio as that for the AEM electrolyte. Hydrophilic PE substrates were immersed in the AEM or CEM electrolyte solution for 1 min, sandwiched using polyethylene terephthalate (PET) films, and photo-cured by a metal-halide lamp (wavelength 365 nm) for 2 min. The PET film was then delaminated, and the membrane surface was polished to remove the unnecessary photopolymerized layer. Patterned membranes were fabricated on the flat membranes using a dispenser-type printer with non-conductive and photo-curable ink with a black pigment. The patterned membranes were designed with wavy lines and mirror images to avoid the overlap of upper and lower patterns. The pattern-to-pattern distance, pattern width, and pattern height were 1.5, 0.4, and 0.1 mm, respectively. Representative images of the CEMs, AEMs, and woven-type spacers used in the actual experiment are presented in Figs. 1 and 4.

### Set-up of RED stack

Two cross-flow-type RED stacks, each consisting of 11 CEMs and 10 AEMs, were used in this study. Stack 1 (flat stack) consisted of flat IEMs with spacers in between them, whereas Stack 2 (pattern stack) consisted of patterned membranes without spacers. Specific information regarding these two stacks is summarized in Table 3. The dimensions, i.e., the effective membrane area of the electrodes was $5 \times 5\ cm^2$. Ti electrodes coated with Ir/Ru (Wesco electrode, South Korea) were used in the RED stack. Polytetrafluoroethylene gaskets reinforced with glass fibers (100 µm thick, Alphaflon, South Korea) were also used. The electrolytes were injected via peristaltic pumps (Cole–Parmer, Masterflex L/S Digital drive, USA) through the stacks at a flow rate of 30 mL/min. ERSs consisting of 50 mM $K_4[Fe(CN)_6]{\cdot}3H_2O$ and 50 mM $K_3[Fe(CN)_6]$ were dissolved in deionized water and recirculated at the same flow rate as the electrolytes between the two electrode compartments.

### Feed waters and RED stack operation

Underground seawater (i.e., lava seawater) originates from the topographic features of volcanic bedrocks. For this study, lava seawater was obtained from the coast of Jeju Island and used owing to its high NaCl concentration. Sewage effluent was obtained from the wastewater treatment plant located on the east coast of Jeju Island and was used as the low-concentration NaCl solution. The ionic compositions of these feed waters are summarized in Supplementary Table 2. Before injecting the two solutions into the RED stack, the sewage effluent was pretreated by filtration using a filter with a 5 µm pore size. The underground seawater was injected into the RED stack without pretreatment. Further, the two feed waters were placed in 200-L tanks, and RED processes were continuously operated, and the pressure at the inlet of the underground seawater and sewage effluent was recorded. The flat stack was operated for 5 days, while the pattern stack was operated for more than 14 days. To prevent overloading the peristaltic pump, the flat stack operation was stopped on the $6^{th}$ day because the pressure on the sewage effluent side remained above 3 bar. Continuous operation was carried out 24 h per day during the experimental period. Switching of the inlet and outlet tubes, which effectively changes the flow direction for in situ cleaning, was performed manually whenever a rise in seawater or sewage pressure of more than 1 bar was observed. However, after 5 days of operation, switching was performed to ensure that the stack pressure remained below 2 bar as much as possible. At pressures above 3 bar, the operation had to be stopped, owing to peristaltic pumping. The pressure drop and flow rate were monitored and recorded every minute using a data logger (GL840, Graphtec Corp., South Korea). Figure 8 shows the simplified scheme and images of the actual experimental setup.

### Characterization of irreversible fouled membranes and RED performance

After the operation, all stacks were disassembled, and surface analysis was conducted. For the surface characterization, the membranes and spacers were rinsed thrice with deionized water and dried in an oven at 80 °C for 24 h. Even though this process can remove reversible fouling, it was conducted to avoid the disruption of the analysis of excess water-soluble inorganic salt compounds (e.g., NaCl). Surface characterization was primarily conducted for the irreversible foulants that remained after cleaning. The surfaces to be characterized were designated as the inlet and outlet regions, which corresponded to 10 mm portions inside the stack. Further, the portion at the center was designated as the middle region (35 mm length). The images of the fouled membranes and spacers were obtained using field-emission (FE) scanning electron microscopy (SEM) (Hitachi, Japan) after the samples were dried. All specimens were Pt-sputtered in a vacuum for 60 s, and during SEM observations, energy dispersive X-ray (EDX, SEM) (Hitachi S-4800, Japan) analysis was further performed to determine the elemental composition of the surfaces.

The chemical structures of the pristine and fouled membranes were analyzed using a Fourier transform infrared (FTIR) spectrometer (FTIR-6300, Jasco, Japan) in the attenuated total reflectance (ATR) mode. Data at a resolution of $2\ cm^{-1}$ in the range 4000–650 $cm^{-1}$ were collected for 128-scans-per-sample.

To measure the area resistance, the fouled membranes were immersed in a 0.5 M NaCl solution for at least 1 day at 24 °C. Thereafter, they were inserted into the flat Pt electrodes (1-cm diameter) of a clip cell in a 0.5 M NaCl solution and their area resistances were measured via impedance spectroscopy using an LCR meter (DU-6011, Delta United Instruments, Taiwan) at a frequency of 1 kHz (Supplementary Fig. 8). To compare the degree of contamination owing to the spacer and the pattern structure, the area resistance of the flat membranes was measured by overlapping a spacer and a flat membrane. After measuring the values corresponding to the electrolyte ($R_s$) and membrane ($R_m$), the membrane resistance was obtained according to the following equation:

$$R = (R_m - R_s) \times A, \quad (1)$$

where A represents the effective membrane area.

The open-circuit voltage (OCV) and the current–voltage (I–V) curve were measured with a linear voltage sweep using a potentiostat (WonA tech., SP2, South Korea) at a scan rate of 10 mV/s. The gross power density was calculated from the maximum I–V curve.

## DATA AVAILABILITY

Data generated during and/or analyzed during this study are included in this article and its supporting information. Raw data are available from the corresponding author on reasonable request.

Received: 16 June 2021; Accepted: 21 January 2022;
Published online: 03 March 2022

## REFERENCES

1. Alvarez-Silva, O. A., Osorio, A. F. & Winter, C. Practical global salinity gradient energy pontential. *Renew. Sust. Energ. Rev.* **60**, 1387–1395 (2016).
2. Guler, E., Zhang, Y., Saakes, M. & Nijmeijer, K. Tailor-made anion-exchange membranes for salinity gradient power generation using reverse electrodialysis. *Chem.Sus.Chem.* **5**, 2262–2270 (2012).
3. Kim, H.-K. et al. High power density of reverse electrodialysis with pore-filling ion exchange membranes and a high open-area spacer. *J. Mater. Chem. A.* **3**, 16302–16306 (2015).
4. Yang, S. et al. R2R fabrication of pore-filling cation-exchange membranes via one-time impregnation and their application in reverse electrodialysis. *ACS. Sustain. Chem. Eng.* **7**, 12200–12213 (2019).
5. Hong, J. G. & Chen, Y. Nanocomposite reverse electrodialysis (RED) ion-exchange membranes for salinity gradient power generation. *J. Membr. Sci.* **460**, 139–147 (2014).
6. Pawlowski, S. et al. Improved fluid mixing and power density in reverse electrodialysis stacks with chevron-profiled membranes. *J. Membr. Sci.* **531**, 111–121 (2017).
7. Güler, E., Elizen, R., Saakes, M. & Nijmeijer, K. Micro-structured membranes for electricity generation by reverse electrodialysis. *J. Membr. Sci.* **458**, 136–148 (2014).
8. Vermaas, D. A., Saakes, M. & Nijmeijer, K. Power generation using profiled membranes in reverse electrodialysis. *J. Membr. Sci.* **385**, 234–242 (2011).
9. Choi, J., Yang, S., Jeong, N. J., Kim, H. & Kim, W. S. Fabrication of an anion-exchange membrane by pore-filling using Catechol–1,4-Diazabicyclo-[2,2,2] octane coating and its application to reverse electrodialysis. *Langmuir.* **34**, 10837–10846 (2018).
10. Tedesco, M. et al. Reverse electrodialysis with saline waters and concentrated brines: A laboratory investigation towards technology scale-up. *J. Membr. Sci.* **492**, 1816–1826 (2015).
11. Tedesco, M. et al. Performance of the first reverse electrodialysis pilot plant for power production from saline waters and concentrated brines. *J. Membr. Sci.* **500**, 33–45 (2016).
12. Di Salvo, J. L., Cosenza, A., Tamburini, A., Micale, G. & Cipollina, A. Long-run operation of a reverse electrodialysis system fed with wastewaters. *J. Environ. Manag.* **217**, 871–887 (2018).
13. Vermaas, D. A. et al. High efficiency in energy generation from salinity gradients with reverse electrodialysis. *ACS Sustain. Chem. Eng.* **1**, 1295–1302 (2013).
14. Hong, J. G. et al. Potential ion exchange membranes and system performance in reverse electrodialysis for power generation: A review. *J. Membr. Sci.* **486**, 71–88 (2015).
15. Mei, Y. & Tang, C. Y. Recent developments and future perspectives of reverse electrodialysis technology: A review. *Desalination* **425**, 156–174 (2018).
16. Jia, Z., Wang, B., Song, S. & Fan, Y. Blue energy: Current technologies for sustainable power generation from water salinity gradient. *Renew. Sustain. Energy Rev.* **31**, 91–100 (2014).
17. Vermaas, D. A., Kunteng, D., Veerman, J., Saakes, M. & Nijmeijer, K. Periodic feedwater reversal and air sparging as antifouling strategies in reverse electrodialysis. *Environ. Sci. Technol.* **48**, 3065–3073 (2014).

18. Moreno, J., De Hart, N., Saakes, M. & Nijmeijer, K. $CO_2$ saturated water as two-phase flow for fouling control in reverse electrodialysis. *Water Res.* **125**, 23–31 (2017).
19. Vermaas, D. A., Kunteng, D., Saakes, M. & Nijmeijer, K. Fouling in reverse electrodialysis under natural conditions. *Water Res.* **47**, 1289–1298 (2013).
20. Nam, J. Y. et al. Assessing the behavior of the feed-water constituents of a pilot-scale 1000-cell-pair reverse electrodialysis with seawater and municipal wastewater effluent. *Water Res.* **148**, 261–271 (2019).
21. Yasukawa, M. et al. Power generation performance of a bench-scale reverse electrodialysis stack using wastewater discharged from sewage treatment and seawater reverse osmosis. *Desalination* **491**, 114449 (2020).
22. Choi, J., Kim, W. S., Kim, H. K., Yang, S. & Jeong, N. J. Ultra-thin pore-filling membranes with wave patterns of mirror images for improved power density and reduced pressure drop in stack of reverse electrodialysis. *J. Membr. Sci.* **620**, 118885 (2021).
23. Vermaas, D. A., Saakes, M. & Nijmeijer, K. Doubled power density from salinity gradients at reduced intermembrane distance. *Environ. Sci. Technol.* **45**, 7089–7095 (2011).
24. Vermaas, D. A., Veerman, J., Saakes, M. & Nijmeijer, K. Influence of multivalent ions on renewable energy generation in reverse electrodialysis. *Energy Environ. Sci.* **7**, 1434–1445 (2014).
25. Pintossi, D., Chen, C.-L., Saakes, M. & Nijmeijer, K. Influence of sulfate on anion exchange membranes in reverse electrodialysis. *npj. Clean. Water* **3**, 29 (2020).
26. Kingsbury, R. S. et al. Impact of natural organic matter and inorganic solutes on energy recovery from five real salinity gradients using reverse electrodialysis. *J. Membr. Sci.* **541**, 621–632 (2017).
27. Zularisam, A. W., Ismail, A. F. & Salim, R. Behaviours of natural organic matter in membrane filtration for surface water treatment — a review. *Desalination* **194**, 211–231 (2006).
28. Cozzolino, A. & Piccolo, A. Polymerization of dissolved humic substances catalyzed by peroxidase. Effects of pH and humic composition. *Org. Geochem.* **33**, 281–294 (2002).
29. Mikhaylin, S. & Bazinet, L. Fouling on ion-exchange membranes: Classification, characterization and strategies of prevention and control. *Adv. Colloid Interface Sci.* **229**, 34–56 (2016).
30. Guo, W., Ngo, H. H. & Li, J. A mini-review on membrane fouling. *Bioresour. Technol.* **122**, 27–34 (2012).
31. Abid, H. S., Johnson, D. J., Hashaikeh, R. & Hilal, N. A review of efforts to reduce membrane fouling by control of feed spacer characteristics. *Desalination* **420**, 384–402 (2017).
32. Salama, W., El Aref, M. & Gaupp, R. Spectroscopic characterization of iron ores formed in different geological environments using FTIR, XPS, Mossbauer spectroscopy and thermoanalyses. *Spectrochim. Acta A Mol. Biomol. Spectrosc.* **136**, 1816–1826 (2015).
33. Zuo, X., Wang, L., He, J., Li, Z. & Yu, S. SEM-EDX studies of $SiO_2$/PVDF membranes fouling in electrodialysis of polymer-flooding produced wastewater: Diatomite, APAM and crude oil. *Desalination* **347**, 43–51 (2014).
34. Wang, P. et al. Amorphous phosphated titanium oxide with amino and hydroxyl bifunctional groups for highly efficient heavy metal removal. *Environ. Sci.: Nano.* **7**, 1266–1274 (2020).
35. Lumsdon, D. G. & Fraser, A. R. Infrared spectroscopic evidence supporting heterogeneous site binding models for humic substances. *Environ. Sci. Technol.* **39**, 6624–6631 (2005).
36. Max, J. J. & Chapados, C. Infrared spectroscopy of aqueous carboxylic acids: Comparison between different acids and their salts. *J. Phys. Chem. A* **108**, 3324–3337 (2004).

## ACKNOWLEDGEMENTS

This research was supported by the Technology Development Program to Solve Climate Changes of the National Research Foundation (NRF) funded by the Ministry of Science, ICT & Future Planning (grant number 2017M1A2A2047366) and the framework of Research and Development Program of the Korea Institute of Energy Research(KIER) (C2-2409).

## AUTHOR CONTRIBUTIONS

J.C.: Conceptualization, Writing-original draft, Investigation, Methodology, W.-S.K.: Investigation, Methodology, Writing-review, H.K.K.: Investigation, Writing-review & editing, S.C. Y.: Methodology, Writing-review and editing, J-H.H. and Y. C. J.: Writing-review and editing, N. J. J.: Funding acquisition, Project administration.

## COMPETING INTERESTS

The authors declare no competing interests.

## ADDITIONAL INFORMATION

**Supplementary information** The online version contains supplementary material available at https://doi.org/10.1038/s41545-022-00149-2.

**Correspondence** and requests for materials should be addressed to Jiyeon Choi or Nam Jo Jeong.

**Reprints and permission information** is available at http://www.nature.com/reprints

**Publisher's note** Springer Nature remains neutral with regard to jurisdictional claims in published maps and institutional affiliations.